Electronic Structure of Metal Clusters. 3. Photoelectron Spectra and Molecular Orbital Calculations on Nonacarbonyltris(μ-hydrido)(μ-alkylidyne)triruthenium

David E. Sherwood, Jr., and Michael B. Hall*

Department of Chemistry, Texas A&M University, College Station, Texas 77843

Received July 7, 1982

Gas-phase, ultraviolet photoelectron (PE) spectra and approximate molecular orbital (MO) calculations are reported for the clusters $(\mu\text{-H})_3Ru_3(CO)_9(\mu_3\text{-CX})$ (X = H, Cl, Br). Comparison of the results with those for $Ru_3(CO)_{12}$ suggests that the Ru–H–Ru interaction is best described as a three-center, two-electron hydrogen bridge without direct Ru–Ru bonds. The Ru–C bonding is best described as an sp-hybridized C, which forms delocalized Ru–C–Ru bonds with the remaining C $2p\pi$ orbitals. The sp "lone pair" on the CX moiety is not delocalized onto the cluster and retains considerable C character. In the related Co clusters $Co_3(CO)_9(\mu_3\text{-CX})$ the highest occupied orbital (HOMO) is involved in the Co–Co bonding while in the Ru clusters the HOMO is mainly Ru–C in character. This difference should be reflected in the chemistry of these species.

Introduction

Recently, Keister[1] synthesized the first nonacarbonyltris(μ-hydrido)(μ_3-alkylidyne)-*triangulo*-triruthenium cluster, $(\mu\text{-H})_3Ru_3(CO)_9(\mu_3\text{-CY})$, **1**, with a chemically activated Y group (Y = OCH_3). Substitution reactions at the apical carbon have opened up an extensive new area of chemistry involving hydrido-bridged *triangulo*-metal clusters. The chemistry is similar to the isoelectronic

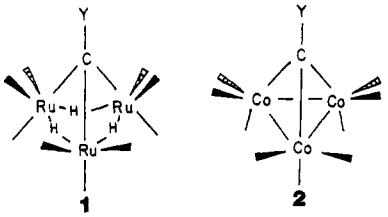

1 **2**

nonacarbonyl(μ_3-alkylidyne)tricobalt clusters, **2**, which have been extensively studied,[2] but the Ru complexes undergo some reaction which have not been observed in the Co systems. Both the hydridoruthenium and the cobalt complexes show large M_3CX^+ and M_3C^+ peaks in the mass spectra[1,2] of the halide derivatives, a result suggesting strong cluster bonding. It has not been determined whether the hydrido hydrogens are still attached to the Ru clusters.

Although many of the general features of the bonding are understood,[3] there remain some questions. One, what is the best description of the carbon–ruthenium bonding? Recently, photoelectron (PE) spectra have been reported for the $Co_3(CO)_9(\mu_3\text{-CY})$ clusters,[4] and our comparison with molecular orbital (MO) calculations indicated that the hybridization of the apical carbon atom is closer to sp than sp^3 with highly delocalized metal to carbon bonds.[4a] Two, to what extent do the bridging hydrides disrupt the metal–metal bonds which are present in the "isoelectronic" *triangulo*-cobalt complexes? Fehlner et al.[4e] recently studied $(\mu\text{-H})_3Fe_3(CO)_9(\mu_3\text{-CCH}_3)$ and its cobalt analogue. They interpreted the PE spectra of these compounds, on going from the Co complex to the Fe complex, as a loss of ionizations due to the metal–metal bonds and a gain in ionizations due to the Fe–H–Fe bonds. They did not comment on the magnitude of any direct Fe–Fe interactions remaining in these Fe–H–Fe bonds. Likewise, Green et al.[5a] compared $Os_3(CO)_{12}$ and $(\mu\text{-H})_3Re_3(CO)_{12}$ and arrived at a similar conclusion. Our recent PE spectra and MO calculations on $Os_3(CO)_{12}$ and $(\mu\text{-H})_2Os_3(CO)_{10}$ suggest some remaining direct Os–Os interaction in this double hydrogen bridge.[6]

To determine the electronic structure of these Ru complexes, we recorded the PE spectra of $(\mu\text{-H})_3Ru_3(CO)_9(\mu_3\text{-CY})$ (Y = H, Cl, Br). These spectra are analyzed by comparison with PE spectra of three related systems: (1) $Ru_3(CO)_{12}$, whose spectrum establishes the positions of the Ru bands in a simple *triangulo*-ruthenium carbonyl cluster, (2) Co analogues whose spectra[4] establish the behavior of the metal–carbon bonds upon substitution of the Y group at the μ_3-carbon, and (3) other complexes containing M–H–M bridges. These results are coupled with Fenske–Hall MO calculations which qualitatively predict the order of the ionizations. Analysis of the molecular orbitals is used to determine which MO's contribute to the Ru–Ru, Ru–C, and Ru-H bonds and to determine the relative strength of these bonds.

Experimental and Theoretical Section

Preparation. All the hydridoruthenium complexes were prepared[1] and kindly given to us by Professor J. B. Keister (SUNY—Buffalo). Ruthenium carbonyl, $Ru_3(CO)_{12}$, was purchased from Strem Chemical Co.

Spectroscopy. The PE spectra were all recorded on a Perkin-Elmer Model PS-18 spectrometer. The total spectrum was recorded as a single slow scan, and the argon $^2P_{3/2}$ and $^2P_{1/2}$ lines

(1) Keister, J. B.; Horling, T. L. *Inorg. Chem.* **1980**, *19*, 2304.
(2) (a) Seyferth, D. *Adv. Organomet. Chem.* **1976**, *14*, 97. (b) Seyferth, D., Eschback, C. S.; Nestle, M. O. *J. Organomet. Chem.* **1975**, *97*, C11. (c) Seyferth, D.; Williams, G. H.; Eschbach, C. S.; Nestle, M. O.; Merola, J. S.; Hallgren, J. E. *J. Am. Chem. Soc.* **1979**, *101*, 4967 and references within the article.
(3) Schilling, B. E.; Hoffmann, R. *J. Am. Chem. Soc.* **1978**, *100*, 6274; **1979**, *101*, 3456.
(4) (a) Chesky, P. T.; Hall, M. B. *Inorg. Chem.* **1981**, *20*, 4419 (Part 1). (b) Costa, N. C. V.; Lloyd, D. R.; Brint, P.; Pelin, W. K.; Spalding, T. R. *J. Chem. Soc., Dalton Trans.* **1982**, 201. (c) Granozzi, G.; Tondello, E.; Ajo, D.; Casarin, M.; Aime, S.; Osella, D. *Inorg. Chem.* **1982**, *21*, 1081. (d) Xiang, S. F.; Bakke, A. A.; Chen, H.-W.; Eyermann, C. J.; Hoskins, J. L.; Lee, T. H.; Seyferth, D.; Withers, H. P., Jr.; Jolly, W. L. *Organometallics* **1982**, *1*, 699. (e) Wong, K. S.; Dutta, T. K.; Fehlner, T. P. *J. Organomet. Chem.* **1981**, *215*, C48.
(5) (a) Green, J. C.; Mingos, D. M. P.; Seddon, E. A. *Inorg. Chem.* **1981**, *20*, 2595. (b) Green, J. C.; Seddon, E. A. Mingos, D. M. P. *J. Chem. Soc., Chem. Commun.* **1979**, 94. (c) Green, J. C.; Mingos, D. M. P.; Seddon, E. A. *J. Organomet. Chem.* **1980**, *185*, C20. (d) Delley, B.; Manning, M. C.; Ellis, D. E.; Berkowitz, J.; Trogler, W. C. *Inorg. Chem.* **1982**, *21*, 2247.
(6) Sherwood, D. E., Jr.; Hall, M. B. *Inorg. Chem.* **1982**, *21*, 3458 (Part 2).

0276-7333/82/2301-1519$01.25/0

at 15.76 and 15.94 eV were used as an internal reference. The resolution for all spectra was better than 30 meV for the fwhm of the Ar $^2P_{3/2}$ peak. The spectrum of $Ru_3(CO)_{12}$ has a low signal to noise ratio because more rapid sublimation at a higher temperature was found to cause substantial decomposition in the spectrometer. Samples of $(\mu\text{-H})_3Ru_3(CO)_9(\mu_3\text{-CY})$ (Y = H, Cl, Br), which are slightly air sensitive, were kept under an Ar atmosphere and loaded into the spectrometer in a glovebag. All spectra were run at the lowest sublimation temperature possible, and even under the mildest conditions some decomposition was noted as a spike in the spectra at the position of free CO (14.05 eV). Only the Y = H derivative was completely stable in the spectrometer.

Theoretical Data. Fenske–Hall MO calculations[7] were performed on an Amdahl 470 V/6 computer at Texas A&M University. The ruthenium basis functions were those of Richardson et al.[8] for Ru 4d[7] and were augmented by a 5s and 5p function with an exponent of 2.20. The carbon, oxygen, and halogen functions were taken from the double-ζ functions of Clementi.[9] An exponent of 1.20 was used for the hydrogen 1s function. Mulliken population analysis was used to determine the individual atomic charges and atomic orbital populations. Overlap populations between atoms were calculated and used to estimate relative bond strengths.

The geometry of the cluster was based on the X-ray crystal structure of the Y = CH_3 derivative of Sheldrick and Yesinowski.[10] The bridging hydrogens were placed below the plane of the Ru_3 atoms on the opposite side from the apical carbon in the manner of Sheldrick and Yesinowski, which was consistent with the NMR work of Buckingham et al.[11] on the methyl derivative. The cluster fragment geometry was idealized to C_{3v} and was fixed at this geometry for all calculations. The C–Y bond distances were taken from standard tables. Our final geometry is very similar to that recently reported for $(\mu\text{-H})_3Ru_3(CO)_9(\mu_3\text{-CCl})$ from a low-temperature crystal structure.[12]

Results and Discussion

Ultraviolet Photoelectron Spectroscopy and Molecular Orbital Calculations of $Ru_3(CO)_{12}$. Although the PE spectrum of $Ru_3(CO)_{12}$ has been discussed previously,[5] it is reproduced and discussed here so that it may be compared to those of $(\mu\text{-H})_3Ru_3(CO)_9(\mu_3\text{-CY})$. Ruthenium carbonyl, **3**, can be viewed as a combination of three

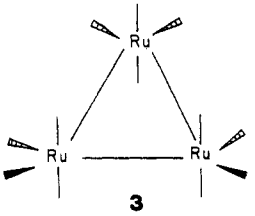

3

pseudooctahedral $Ru(CO)_4$ fragments. The results of Fenske–Hall molecular orbital calculations on $Ru(CO)_4$ and $Ru_3(CO)_{12}$ were used to produce the molecular orbital diagram shown in Figure 1. The MO indexing begins with the first orbital which is higher in energy than the C $5\sigma \rightarrow$ M d_σ bonds.

First, we consider the isolated $Ru(CO)_4$ fragment (left side of Figure 1). The orbitals can roughly be grouped into three sets: a pseudo-t_{2g} set containing the three metal orbitals which have lobes pointing off the Ru–C internuclear axis and are stabilized by M $d_\pi \rightarrow$ CO 2π back-donation, a pseudo-e_g set containing the two metal orbitals which have lobes pointing along the Ru–C internuclear axis

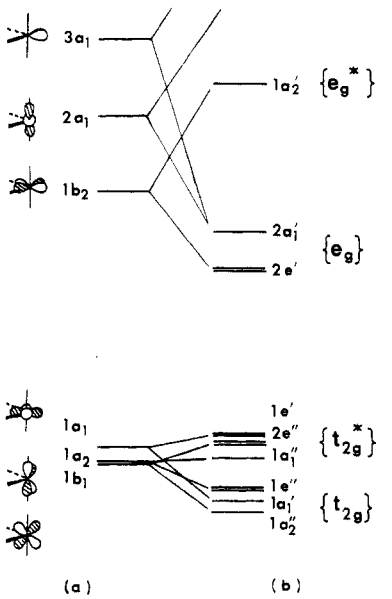

Figure 1. Molecular orbital diagram for the formation of $Ru_3(CO)_{12}$ from three $Ru(CO)_4$ fragments. The relative separation of molecular orbitals is based on the results of Fenske–Hall molecular orbital calculations.

and are destabilized by C $5\sigma \rightarrow$ M d_σ donation, and a pseudo-a_{1g} orbital which is primarily Ru 5s and 5p in character. The calculated splitting among the pseudo-t_{2g} levels is small, they are all doubly occupied, and the pseudo-t_{2g} electrons can be described as Ru "lone pairs". The "t_{2g}–e_g" splitting ($10Dq$) is large, a result which is consistent with the large crystal field splitting of the CO ligand and the second transition-series metal, Ru. Within the pseudo-e_g set the $1b_2$ orbital is lower in energy than the $2a_1$ orbital because the $1b_2$ orbital is destabilized by only two carbonyl donors, whereas the $2a_1$ orbital is destabilized by four carbonyl donors. The pseudo-e_g orbitals contain a total of two electrons in the neutral $Ru(CO)_4$ fragment. The pseudo-a_{1g} orbital ($3a_1$), which is metal in character, is at higher energy because it is composed mainly of Ru 5s and 5p atomic orbitals.

When three $Ru(CO)_4$ fragments are brought together to form the united $Ru_3(CO)_{12}$ molecule, there will be little mixing between the pseudo-t_{2g} orbitals and the pseudo-e_g orbitals because the "t_{2g} – e_g" splitting is large for $Ru(CO)_4$. The pseudo-t_{2g} orbitals form a bonding set, $\{t_{2g}\}$, and an antibonding set, $\{t_{2g}^*\}$, with respect to metal–metal bonding. Fenske–Hall calculations predict the ratio of orbitals $\{t_{2g}\}/\{t_{2g}^*\}$ to be 4/5 with a small splitting between them. Since all of these pseudo-t_{2g} levels are doubly occupied, they contribute little to the metal–metal bonds.

The orbitals lying along the Ru–Ru internuclear axis are mainly derived from the pseudo-e_g orbitals of the $Ru(CO)_4$ fragments. These form a bonding set, $\{e_g\}$, which is totally occupied and an antibonding set, $\{e_g^*\}$, which is unoccupied. The bonding $\{e_g\}$ transform as two degenerate orbitals which are combinations of the $Ru(CO)_4$ fragment $1b_2$ orbitals, **4**, and a nondegenerate orbital which is a symmetric combination of fragment $2a_1$ and $3a_1$ orbitals, **5**. The

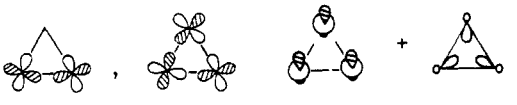

4 **5**

orbital shown in **5** is predicted to be the highest occupied molecular orbital (HOMO), preserving the $1b_2$ – $2a_1$ splitting of the $Ru(CO)_4$ fragment orbitals. There is also

(7) Hall, M. B.; Fenske, R. F. *Inorg. Chem.* **1972**, *11*, 768.
(8) Richardson, J. W.; Blackman, M. J.; Ranochak, J. E. *J. Chem. Phys.* **1973**, *58*, 3010.
(9) Clementi, E. *IBM J. Res. Dev.* **1965**, *9*, 2.
(10) Sheldrick, G. M.; Yesinowski, J. P. *J. Chem. Soc., Dalton Trans.* **1975**, 873.
(11) Buckingham, A. D.; Yesinowski, J. P.; Canty, A. J.; Rest, A. J. *J. Am. Chem. Soc.* **1973**, *95*, 2732.
(12) Zhu, N. J.; Lecomte, C.; Coppens, P.; Keister, J. B. *Acta Crystallogr., Sect. B* **1982**, *B38*, 1286.

Table I. Ionization Energies (eV) (±0.05)

molecule	band I	II	III	IV	V	VI
$Ru_3(CO)_{12}$	8.0	8.3	9.5	10.2		
$(\mu\text{-}H)_3Ru_3(CO)_9(\mu_3\text{-}CH)$	8.3	8.6	9.5	10.75	11.8	13.05
$(\mu\text{-}H)_3Ru_3(CO)_9(\mu_3\text{-}CCl)$	8.2	8.5	9.45	10.5	12.1[a]	13.3
$(\mu\text{-}H)_3Ru_3(CO)_9(\mu_3\text{-}CBr)$	7.95	8.4	9.4	10.2	11.7[a]	12.9

[a] Weighted average.

a significant amount of Ru 5s and 5p bonding character in the HOMO. The ratio of orbitals within the $\{e_g\}$ is 1/2. The calculations predict that the splitting within the $\{e_g\}$ is small compared to the $\{e_g\}$ – $\{t_{2g}^*\}$ splitting.

With these results in mind it is relatively easy to interpret the PE spectra of $Ru_3(CO)_{12}$ (Figure 2a). The four bands between 8.0 and 11.0 eV are the ionizations from the manifold of metal orbitals. The CO 5σ and 1π ionizations begin at ~13 eV. Band IV arises from ionizations of the $\{t_{2g}\}$, and band III arises from ionizations of the $\{t_{2g}^*\}$. Both bands have similar intensities, as predicted, and are separated by about 1.0 eV. Bands I and II corresponds to ionizations from the $\{e_g\}$. The stronger peak at higher ionization energy (IE), II, corresponds to the doubly degenerate $\{e_g\}$ orbitals (4e). The lowest IE peak, I, is the totally symmetric bonding combination of the $\{e_g\}$ set ($3a_1$). The $\{e_g\}$ ionizations are well separated from the $\{t_{2g}^*\}$ and $\{t_{2g}\}$ ionizations, as predicted.

No attempt will be made to assign the features within the $\{t_{2g}\}$ or $\{t_{2g}^*\}$ sets of ionizations, because there are several closely spaced orbitals within each manifold. Our assignments of the PE spectra $(\mu\text{-}H)_3Ru_3(CO)_9(\mu_3\text{-}CY)$ (Y = H, Cl, Br) will be based on the general features described above.

Electronic Structure and Ultraviolet Photoelectron Spectrum of $(\mu\text{-}H)_3Ru_3(CO)_9(\mu_3\text{-}CH)$. The PE spectrum of $(\mu\text{-}H)_3Ru_3(CO)_9(\mu_3\text{-}CH)$ is shown in Figure 2b and will be described with reference to the parent carbonyl (Figure 2a). Two new bands (V and VI) appear in the high IE region of the spectrum. Only band VI is observed in some of the analogous Co spectra,[4] and this was assigned to ionizations of an orbital with a high percentage of methylidyne character. The other new band, band V in Figure 2b, occurs at the position found for M–H–M ionizations in several complexes with hydrido-bridged metal–metal bonds.[4-6] Band IV appears at a slightly higher IE than the $\{t_{2g}\}$ band of $Ru_3(CO)_{12}$. Band III appears at a slightly lower IE than the $\{t_{2g}^*\}$ band of $Ru_3(CO)_{12}$. Presumably, bands III and IV contain some similar pseudo-t_{2g} $Ru(CO)_3$ fragment orbital interactions, but band III is now much more intense than band IV. In the cobalt analogues, ionizations from an orbital involved the bond between the cobalt atoms and the C 2p orbitals have been assigned to a peak slightly higher in IE than the Co lone-pair ionizations. Thus, band IV may contain considerable C character. Bands I and II appear similar to those of the parent carbonyl, but as will be shown, they are very different in character.

Although the hydridoruthenium alkylidyne complex is closely related to the parent carbonyl, the electronic structure is substantially more complex. In order to examine the bonding, we developed a hypothetical scheme for the formation of $(\mu\text{-}H)_3Ru_3(CO)_9(\mu_3\text{-}CH)$ from $Ru_3(CO)_{12}$ in a stepwise manner. One can view this cluster as the replacement of three CO moieties from $Ru_3(CO)_{12}$ by a CH^{3-} cap, which would have three electron pairs to donate to the three Ru atoms. Then the three bridging hydrogens can be thought of as H^+ fragments which protonate the cluster.

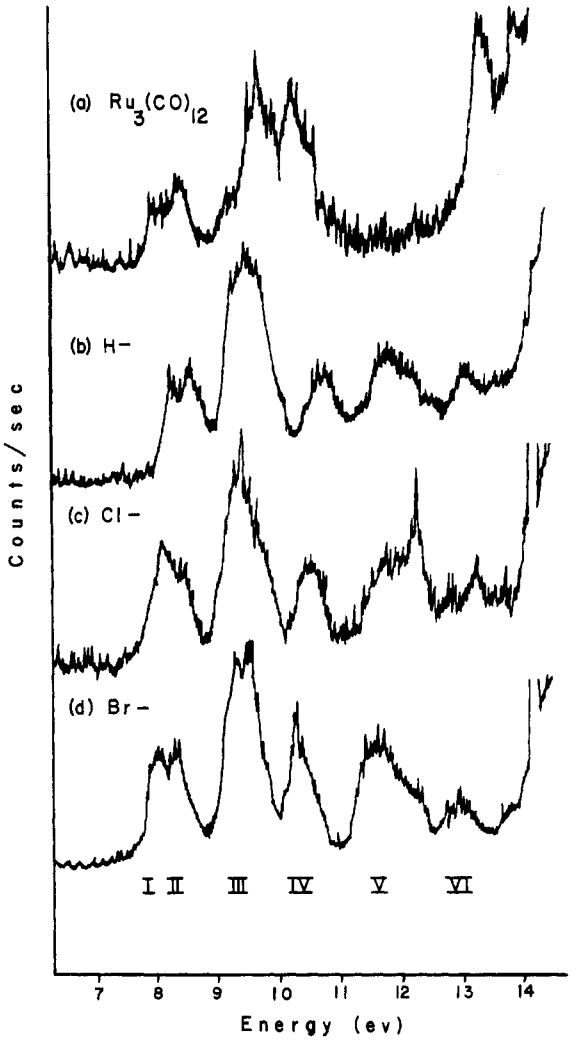

Figure 2. Ultraviolet photoelectron spectra of (a) $Ru_3(CO)_{12}$ and the substituted nonacarbonyl alkylidyne clusters $(\mu\text{-}H)_3Ru_3(CO)_9(\mu_3\text{-}CX)$, with (b) X = H, (c) X = Cl, and (d) X = Br.

The MO diagrams for building the cluster in this fashion are shown in Figure 3. The MO diagram for $Ru_3(CO)_{12}$ has the experimental IE's plotted with the assignments given from the MO calculations. When three CO moieties are removed and the remaining carbonyl groups are placed at the positions found in the alkylidyne complex, the hypothetical $Ru_3(CO)_9$ species preserves the orbital distribution found in the PE spectrum of $Ru_3(CO)_{12}$, the pattern $\{t_{2g}\}$, $\{t_{2g}^*\}$, and $\{e_g\}$. The calculations predict an interchange of the 4e and $3a_1$ orbitals and the appearance of a low-energy acceptor orbital, 5e. The latter was previously used to accept electrons from the three CO's.

The molecular orbital diagram for $[Ru_3(CO)_9(\mu_3\text{-}CH)]^{3-}$ is given in the third column of Figure 3. The three lone-pair orbitals of CH^{3-} transform as an a_1 (C), which points in the direction of the midpoint of the Ru_3 triangle, and a degenerate e(C) set, which is the filled $2p_\pi$ orbitals on the C atom. The a_1(C) orbital interacts strongly with the

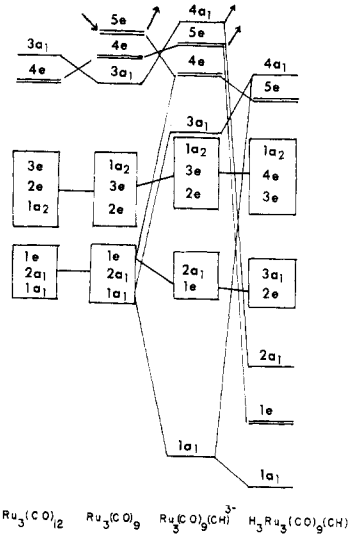

Figure 3. Molecular orbital diagrams for the stepwise formation of $(\mu\text{-H})_3Ru_3(CO)_9(\mu_3\text{-CH})$ from $Ru_3(CO)_{12}$. See text for a detailed discussion.

$1a_1$ of the $\{t_{2g}\}$ of $Ru_3(CO)_9$ forming a bonding combination, the $1a_1$ orbital of $[Ru_3(CO)_9(\mu_3\text{-CH})]^{3-}$, and an antibonding combination, the $3a_1$ orbital of the trianion. The bonding combination is mostly carbon "lone pair" in character and would occur at a high IE. The Ru–C antibonding orbital, the $3a_1$, although Ru–Ru t_{2g} bonding, is pushed up into the $\{t_{2g}^*\}$ region. The C lone pair also interacts with the $3a_1$, the Ru–Ru bonding orbital formed from the pseudo-e_g orbitals of the Ru fragment, and pushes it to lower IE. A similar interaction occurs with the C $2p_\pi$ orbitals, which interact with the 1e orbital of the $Ru_3(CO)_9$ $\{t_{2g}\}$, forming bonding and antibonding combinations. The bonding combinations, the 1e of $[Ru_3(CO)_9(\mu_3\text{-CH})]^{3-}$, is mainly C $2p_\pi$ in character. The antibonding combination, the 4e, is destabilized to such an extent, that it is now among the pseudo-e_g orbitals. The 4e orbital also mixes in a substantial amount of the 5e orbital of $Ru_3(CO)_9$ and thus has some Ru–C bonding interaction between the C $2p_\pi$ and Ru pseudo-e_g orbitals.

The molecular orbital diagram for $(\mu\text{-H})_3Ru_3(CO)_9(\mu_3\text{-CH})$ is shown at the right in Figure 3. The energies are those found in the PE experiment, and the assignments are based on the results of MO calculations on the complex. The $\{e_g\}$ Ru–Ru bonds of $[Ru_3(CO)_9(\mu_3\text{-CH})]^{3-}$ ($4a_1$ and 5e) disappear because they are used in the Ru–H bonding orbitals, the 1e and the $2a_1$ of $(\mu\text{-H})_3Ru_3(CO)_9(\mu_3\text{-CH})$. (The Ru–C interactions are essentially the same as before protonation.) The symmetric combination of H orbitals interacts with the $1a_1$, $3a_1$, and $4a_1$ orbitals of the trianion, producing the $1a_1$, $2a_1$, and $4a_1$ orbitals. The $1a_1$ orbital is still mostly a Ru–C bonding orbital, while the $2a_1$ orbital is mainly Ru–H bonding in character. The $4a_1$ is antibonding between the Ru pseudo-t_{2g} and both H and C and is destabilized to such an extent that it is now the HOMO. The 1e and 4e orbitals of the trianion interact to a small extent with the e combination of H atomic orbitals causing some t_{2g}–e_g mixing in the 1e, 2e, and 5e orbitals of $(\mu\text{-H})_3Ru_3(CO)_9(\mu_3\text{-CH})$. The 1e orbitals are mainly the (H–$\{e_g\}$) bonding orbitals which have a very small amount of (H–$\{t_{2g}\}$) character. The 2e is mainly (C $2p_\pi$–$\{t_{2g}\}$). The 5e has a very small amount of (H–$\{t_{2g}\}$) antibonding character but remains mainly the bonding combination of C $2p_\pi$ orbitals and Ru pseudo-e_g orbitals.

Now, the spectrum of $(\mu\text{-H})_3Ru_3(CO)_9(\mu_3\text{-CH})$ can be assigned in detail (IE values in Table I). Band V is the ionization of the stabilized carbon "lone-pair" orbital, the

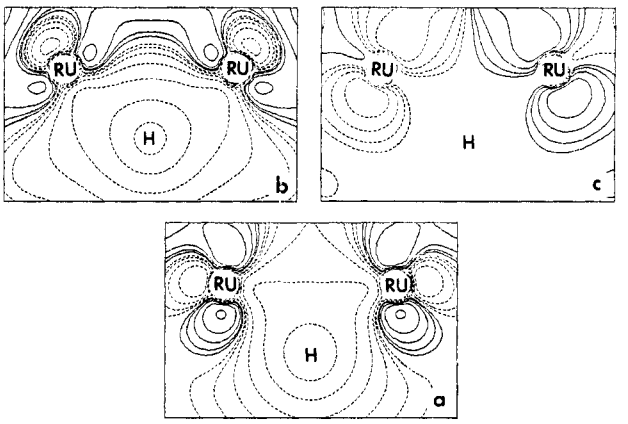

Figure 4. Molecular orbital plots in the Ru–H–Ru plane of the ruthenium hydrogen bonding orbitals in $(\mu\text{-H})_3Ru_3(CO)_9(\mu_3\text{-CH})$. Part a is the totally symmetric $2a_1$ orbital, and parts b and c are plots of the two orthogonal components of the 1e.

$1a_1$. Band V is the three M–H–M bonding orbitals, the 1e and $2a_1$. Band IV is the (C $2p_\pi$–$\{t_{2g}\}$) bonding orbital, the 2e, and the remaining $\{t_{2g}\}$ orbital, the $3a_1$. Band III is the $\{t_{2g}^*\}$. Band II contains some (C $2p_\pi$–$\{t_{2g}\}$) antibonding character but is principally a (C 2p–$\{e_g^*\}$) bonding orbital, the 5e. Band I, due to the $4a_1$ orbital, is mainly a $\{t_{2g}\}$ orbital which is antibonding with respect to Ru–C and Ru–H interactions.

Molecular Orbitals of $(\mu\text{-H})_3Ru_3(CO)_9(\mu_3\text{-CH})$. In order to better understand the bonding in $(\mu\text{-H})_3Ru_3(CO)_9(\mu_3\text{-CH})$, we have made orbital plots of the important Ru–C and Ru–H bonding orbitals. Solid contours and dashed contours represent positive and negative values of the wave function, respectively. The main Ru–H–Ru MO's are plotted in Figure 4. Both the $2a_1$ and 1e orbitals are more Ru–H character than Ru–Ru character because more contours are crossed in the Ru–H direction than in the Ru–Ru direction. One of the 1e orbitals (Figure 4c) has a node at this H but is bonding in the other two Ru–H–Ru planes. The other 1e orbital (Figure 4b) looks like of an open three-center, two-electron (3-c, 2-e) bond as the hybrid on Ru is directed at the H. There is little direct Ru–Ru bonding in the 1e as the contour along the Ru–Ru direction is one-eighth of the maximum around H. The $2a_1$ is somewhat different as the hybrid on Ru is directed more toward the other Ru than the H. Thus, this component looks more like a closed 3-c, 2-e bond. The contour along the Ru–Ru direction is half of the maximum around H, and the $2a_1$ retains some Ru–Ru bonding. In a qualitative description one would usually assume that the same hybrids on Ru would be used for both the $2a_1$ and 1e. They are not. At the simplest level the system would be described correctly as three 3-c, 2-e Ru–H–Ru bonds without a direct Ru–Ru bond. However, because of the bridging H can stabilize the in-phase combination of Ru–Ru interactions, there remains some degree of net Ru–Ru bonding. This result is even more dramatic in the double H bridge of $(\mu\text{-H})_2Os_3(CO)_{10}$.[6]

The Ru–C interactions are more complicated, and in order to display the interactions within a single orbital, we have plotted three planes. One plane contains Ru and C atoms and slices through the center of the Ru_3C tetrahedron. Since this plane contains the region from the midpoint of the Ru_3 triangle to the apical carbon, it will be referred to as the interior plane. Although this plane shows the Ru–C bond, we have also plotted the perpendicular plane which contains the Ru–C edge of the polyhedron. This plane will be referred to as the edge plane. The third plane contains the other two ruthenium atoms

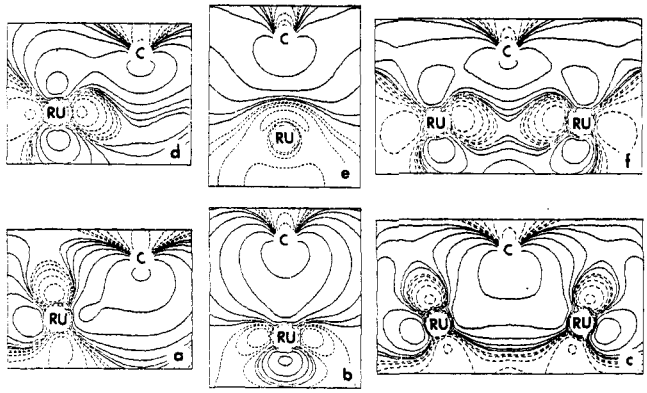

Figure 5. Molecular orbital plots for the two orbitals with strong C sp–Ru t_{2g} interactions. Three planes are shown for each orbital. From left to right the planes are the following: a plane which passes through the interior of the Ru_3C tetrahedron (interior plane), a plane perpendicular to the first and containing the Ru and C atoms (edge plane), and the Ru_2C plane on the opposite face of the Ru_3C tetrahedron (face plane). Parts a–c are for the bonding $1a_1$ orbital. Parts d–f are for the $4a_1$ orbital.

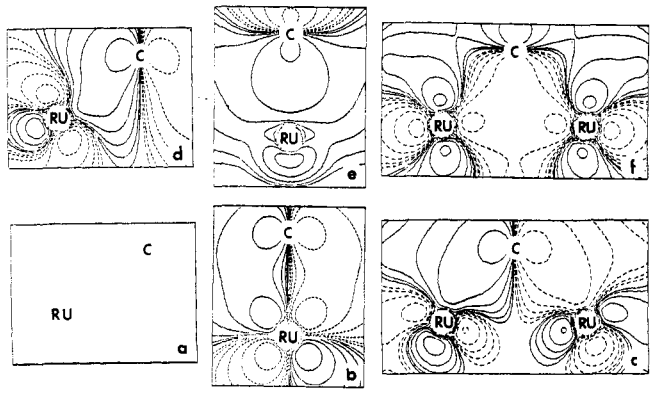

Figure 6. Molecular orbital plots for the two orthogonal components of the 2e orbital. The planes and contouring are identical with those of Figure 5.

and the carbon atom. This face of the Ru_3C "tetrahedron" is opposite the Ru–C edge-bond for each orbital shown and will be referred to as the face plane.

The C "lone-pair" orbital interacts strongly with one of the symmetric combinations of Ru pseudo-t_{2g} orbitals in the $\{t_{2g}\}$ and forms the very stabilized $1a_1$ orbital and the very destabilized $4a_1$ orbital. These orbitals are shown in Figure 5. The plots of the $1a_1$ in parts a, b, and c of Figure 5 (the interior, edge, and face planes, respectively) all show bonding Ru–C interactions. The corresponding plots of the $4a_1$ in parts d, e, and f of Figure 5 show an antibonding interaction between the same Ru 4d orbital and the C "lone-pair" orbital. The C "lone pair" is too stable to interact effectively with the pseudo-e_g orbitals on each $Ru(CO)_3$. Thus, there is little net donation from this C "lone pair" and only weak Ru–C bonding from the MO's of a_1 symmetry.

The two sets of doubly degenerate e orbitals, 2e and 5e, involved in the Ru–C bonds are shown in Figures 6 and 7, respectively. The 2e orbitals represent bonding of the C $2p_\pi$ orbitals with the Ru pseudo-t_{2g} orbitals $\{t_{2g}\}$. One orbital of the 2e set has a nodal plane which passes through the interior of the Ru_3C cluster. This orbital has an interior map that is zero everywhere (Figure 6a). As can be seen from the edge map (Figure 6b), this is a Ru $4d_\pi$–C $2p_\pi$ π bond in the sense that there is a node along the Ru–C internuclear axis. However, the other two Ru atoms are bonding in a σ manner on the opposite face (Figure 6c). The other component of the 2e shows a Ru–C σ interaction

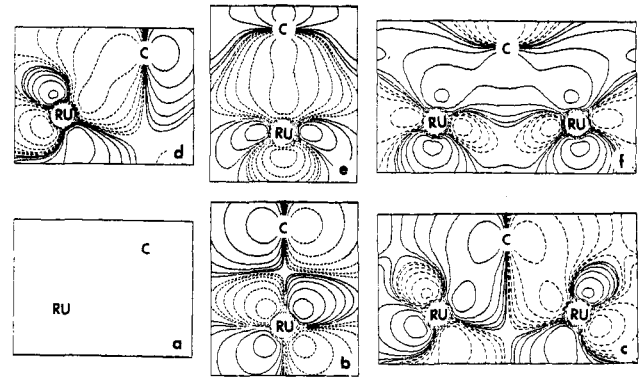

Figure 7. Molecular orbital plots for the two orthogonal components of the 5e orbital. The planes and contouring are identical with those of Figure 5.

through the interior which is localized toward the carbon atom (parts d and e of Figure 6). The opposite Ru_2C face (Figure 6f) contains a delocalized face bonding orbital.

The 5e orbital (Figure 7) represents an antibonding (C $2p_\pi$–Ru $\{t_{2g}\}$) interaction and a bonding (C 2p–$\{e_g^*\}$) interaction; overall the orbitals are Ru–C bonding but Ru–Ru antibonding. One of the 5e orbitals has a nodal plane through the interior, and the interior map (Figure 7a) is zero everywhere. The edge of this orbital is Ru $4d_\pi$–C $2p_\pi$ antibonding (Figure 7b) which negates the bonding of Figure 6b. The bonding on the opposite face (Figure 7c) is Ru–C $2p_\pi$ σ bonding. This is predominantly bonding of the C with the pseudo-e_g orbitals of the Ru atoms from the $\{e_g^*\}$ set. In this face the 45° rotation of the metal orbitals from those in Figure 6c is apparent. The other orthogonal component of the 5e set is strongly bonding along the Ru–C axis (parts d and e of Figure 7) and is a more equal mixture of Ru and C than the 2e (parts d and e of Figure 6). The face interaction in Figure 7f is the antibonding counterpart of the face interaction in Figure 6f. The 2e orbital (Figure 6) is both σ and π bonding along the edge and bonding in all faces. The 5e orbital enhances the σ edge bonding but serves to cancel the π edge bond and some of the facial bonding. The net bonding interactions involve a Ru orbital pointed directly at the C atom which is trans to a CO and are best described as two "3-c, 2-e" Ru–C–Ru bonds formed from the $Ru_3(CO)_9$ $\{e_g^*\}$ and C $2p_\pi$ orbitals.

Some overall conclusions can be drawn from the orbital plots just presented and the calculated overlap populations of the Ru–Ru, Ru–C, and Ru–H bonds. Although the pseudo-t_{2g} orbitals of the $Ru(CO)_3$ groups interact with the C $2p_\pi$ orbitals, carbon lone-pair orbital, and symmetric combination of H orbitals, there is little net Ru–C or Ru–H bonding from this set because their antibonding counterparts are also filled. On the basis of overlap populations between the Ru 4d orbitals and the ligand orbitals, the Ru–H bonds are 97% with the pseudo-e_g orbitals and the Ru–C bonds are 96% with the pseudo-e_g orbitals. The direct Ru–Ru bonding interaction is small. On going from $Ru_3(CO)_{12}$ to $[Ru_3(CO)_9(\mu_3\text{-}CH)]^{3-}$ the overlap populations between the Ru 4d orbitals decreases by 30%. This is because the 5e orbital of $Ru_3(CO)_9$, a member of the $\{e_g^*\}$ is used for bonding with the C $2p_\pi$ orbitals. Upon protonation, the Ru–Ru 4d overlap populations are reduced an additional 64% because the 4e of $Ru_3(CO)_9$ is used to form the Ru–H–Ru bonds. Hence, only about 6% of the Ru 4d–Ru 4d bonding interaction is left compared with $Ru_3(CO)_{12}$. While calculations at this level are only approximate and overlap populations can be misleading, it is clear that the H atoms seriously disrupt the metal–metal

bonds compared with the parent molecule or the isoelectronic (valence electrons) $Co_3(CO)_9(\mu_3\text{-}CH)$.

Electronic Structure and Photoelectron Spectra of $(\mu\text{-}H)_3Ru_3(CO)_9(\mu_3\text{-}CX)$ (X = Cl, Br). The electronic structure of the halogen derivatives will be complicated only by the presence of the halogen "lone pairs". The halogen "lone-pair" orbitals form a doubly degenerate e combination. The Cl "lone pairs" are more stable and should appear at a higher IE than the C $2p_\pi$ orbitals. Since they are of the same symmetry as the C $2p_\pi$ orbitals, they will interact with the same $Ru_3(CO)_9$ fragment orbitals and will destabilize the orbitals with C $2p_\pi$ character. Hence, one expects that the orbitals in the halo derivatives, which correspond to the 2e and 5e of the hydrido derivative, will be pushed to lower IE. The halogen "lone pairs" may be strongly delocalized into the clusters.

The PE spectrum of the chloro derivative is shown in Figure 2c. The new peak in band V (12.2 eV) corresponds to the Cl $3p_\pi$ ionizations. Band IV, which corresponds to the 2e in hydrido derivatives, is pushed 0.25 eV to lower IE. Band II, which corresponds to the 5e orbital of $(\mu\text{-}H)_3Ru_3(CO)_9(\mu_3\text{-}CH)$ is pushed 0.4 eV to the lowest IE and is now the HOMO. This assignment is made because the relative intensity of the bands changes from 1/2 in the hydrido complex to 2/1 in the chloro complex and because the bands arising from e ionizations should be affected more strongly than the other bands due to interactions with the chlorine lone pairs. As is often the case, the HOMO is most sensitive to the perturbation.

The PE spectrum of $(\mu\text{-}H)_3Ru_3(CO)_9(\mu_3\text{-}CBr)$ is shown in Figure 2d. Bromine lone pairs are less stable than chlorine lone pairs (the IE becomes lower as one goes down a column in the periodic table). In band V the lone pair ionizations move from the high IE side in the Cl derivative to the low IE side in the Br derivative. Similarly, the C $2p_\pi$ ionizations, which correspond to the 2e, move to the leading edge of band IV and gain intensity from Br contributions. Band I moves to a slightly lower IE, whereas band II does not move from its position in the chloro derivative, a result which is consistent with the assignment of band I to an e orbital analogous to the 5e orbital of $(\mu\text{-}H)_3Ru_3(CO)_9(\mu_3\text{-}CH)$.

Conclusions. The combination of PE spectra and MO calculations provides an internally consistent description of the bonding in the $(\mu\text{-}H)_3Ru_3(CO)_9(\mu_3\text{-}CX)$ systems. The Ru–H bonding is best described as three three-center, two-electron bonds, which use the pseudo-e_g orbitals $\{e_g\}$. The Ru–C bonding consists of a weak bond with carbon "lone-pair" donation to the symmetric orbital of the $\{e_g\}$ and two degenerate bonds formed from the degenerate $\{e_g^*\}$ and C $2p_\pi$ orbitals. The direct metal–metal interaction is weak because the bonding and antibonding combinations of metal orbitals are employed in Ru–C and Ru–H bonding. The orbitals, which would be metal–metal bonding, $\{e_g\}$, are now metal–ligand bonding and not available for metal–metal bonding.

A remaining question is how to describe the hybridization of the apical carbon atom. We have seen from the molecular orbital plots that there is no net π bonding in the Ru to C bond since orbitals with nodes along the Ru–C internuclear axis cancel. There are, however, $Ru_3(CO)_9$ $\{e_g^*\}$–C $2p_\pi$ bonds, which are σ in nature since they are directed along the Ru–C axis, but involve a C π-type orbital. The question of hybridization really involves the degree of donation from the C "lone pair" or equivalently the amount of C 2s character in the Ru–C bonds. Since both the Ru–C "lone-pair" bonding ($1a_1$) and antibonding ($4a_1$) MO's are occupied, their is little net donation and the Ru–C bonds are primarily 2p in character. Thus, as in $Co_3(CO)_9(\mu_3\text{-}CX)$, the hybridization at C is closer to sp than sp^3.

In spite of the similarity of $Co_3(CO)_9(\mu_3\text{-}CX)$ and $(\mu\text{-}H)_3Ru_3(CO)_9(\mu_3\text{-}CX)$ there are some important differences in the electronic structure. One difference is related to the tilt of the $M(CO)_3$ fragments. In the Co clusters, two CO's of the $Co(CO)_3$ fragment are trans to Co–Co bonds, **6**. The

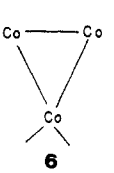

6

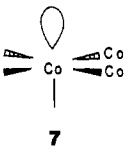

7

remaining CO is almost perpendicular to the Co_3 plane, **7**. This means that a Co pseudo-t_{2g} orbital points toward the apical carbon and not a pseudo-e_g orbital. In the Ru clusters, two CO's of the $Ru(CO)_3$ cluster are trans to the Ru–H bonds which are below the Ru_3 plane, **8**. The remaining CO whose position is such as to preserve pseudooctahedral symmetry is now *trans* to the apical C, **9**.

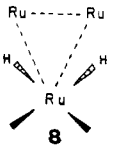

8

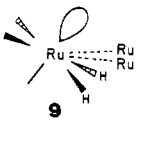

9

Thus, there is a pseudo-e_g orbital directed at the apical carbon. In both systems M–C bonds are formed mainly with the pseudo-e_g set. The orbital which is (C $2p_\pi$–$\{e_g^*\}$) bonding in the Co clusters shows a bent bond outside the Co_3C "tetrahedron",[4a] while that in the Ru clusters is directed along the Ru_3C edge (Figures 6 and 7).

Although relatively few comparisons of first and second-row transition metals have been made with Fenske–Hall MO calculations, our results suggest a significant difference between the HOMO of the Ru and Co clusters. In the Co clusters the HOMO is involved primarily in Co–Co bonding, while in the Ru clusters it is involved primarily in the Ru–C interaction. This difference should be reflected in the chemistry of these and related systems such as the cations $Co_3(CO)_9(CCHR)^{+}$[2c] and $(\mu\text{-}H)_3Os_3(CO)_9(CCHR)^{+}$.[13]

Acknowledgment. We thank the Robert A. Welch Foundation (Grant A-648) and the National Science Foundation (Grant CHE 79-20993) for support of this work. Professor J. B. Keister (SUNY—Buffalo) kindly provides the samples for this study.

Registry No. $Ru_3(CO)_{12}$, 15243-33-1; $(\mu\text{-}H)_3Ru_3(CO)_9(\mu_3\text{-}CH)$, 63280-43-3; $[Ru_3(CO)_9(\mu_3\text{-}CH)]^{3-}$, 83026-04-4; $(\mu\text{-}H)_3Ru_3(CO)_9(\mu_3\text{-}CCl)$, 73746-97-1; $(\mu\text{-}H)_3Ru_3(CO)_9(\mu_3\text{-}CBr)$, 73746-95-9; Co, 7440-48-4.

(13) Deeming, A. J.; Hasso, S.; Underhill, M.; Canty, A. J.; Johnson, B. F. G.; Jackson, W. G.; Lewis, J.; Matheson, T. W. *J. Chem. Soc., Chem. Commun.* **1974**, 807.